Tutor/s

Dr. Alessandro Sorrenti
Departament de Química Inorgànica I Orgànica

James Nicholas
Departament de Ciència de Materials I Química Física

Grau de Química

Treball Final de Grau

Dissipative self-assembly of redox-responsive porous supramolecular networks.
Autoensamblaje disipativo de redes supramoleculares con respuesta redox.

María Camacho Molina

June 2023

UNIVERSITAT DE BARCELONA

B:KC Barcelona Knowledge Campus
Campus d'Excel·lència Internacional

Soy de las que piensan que la ciencia tiene una gran belleza. Un científico en su laboratorio no es sólo un técnico: también es un niño colocado ante fenómenos naturales que lo impresionan como un cuento de hadas.

Marie Curie

Me gustaría agradecer a Alessandro por ayudarme y enseñarme durante todo el proyecto, por preocuparse y por hacerme reír siempre. Por hacer que disfrute del trabajo en el laboratorio y por ser un gran apoyo.

A James por ayudarme siempre que lo necesitaba, por sacarme siempre una sonrisa y por entenderme cuando intentaba hablar en inglés.

A las chicas por apoyarme, por estar cuando las necesitaba y por hacerme reír en nuestras horas de charla en el comedor.

A mi madre, mi hermano y mis amigos por ser un soporte siempre, entenderme y aguantar mi mal humor.

REPORT

IDENTIFICATION AND REFLECTION ON THE SUSTAINABLE DEVELOPMENT GOALS (SDGs)

To find solutions to solve the major problems facing the world today, in 2015, the United Nations created a list of 17 Sustainable Development Goals (SDGs) that are grouped into five broad blocks, known as the 5Ps. As responsible research scientists, we must consider how our work can help to pursue some of these goals.

In the area of porous systems, some of these objectives can be addressed, for example, in the design of new drug delivery systems. The application of non-equilibrium self-assembly behaviour in these systems, with the ability to control the state of assembly in space and time, can bring innovative therapeutic solutions, thus pointing to SDG 3 (good health and well-being), within the People area of the 5Ps.

Dissipative self-assembly (DSA) systems require an energy supply by means of chemical fuels, a part of the energy is dissipated in the form of waste, understanding the conversion cycles could regulate energy consumption and waste formation and thus make the process more sustainable in line with SDG 12 (responsible consumption and production), within the 5Ps Planet area.

Following SDG 7 (affordable and clean energy) within the 5Ps Prosperity area, the supramolecular polymeric structures developed in this TFG could give rise to new light-harvesting materials, because they are formed from porphyrins, and thus are ordered arrays of chromophores. It could therefore target the described objective of capturing solar energy as a clean energy source.

Contents

1. SUMMARY

Porous materials, such as Metal-Organic Frameworks (MOFs), Covalent-Organic frameworks (COFs), and Supramolecular Organic Frameworks (SOFs), are of great scientific interest for a variety of applications such as molecular recognition, sensing, transport, separation, and catalysis. MOFs and COFs are crystalline materials, showing porosity in the solid state, and they are typically insoluble and/or instable in solution, which hampers their applications in homogeneous media. In contrast, SOFs are soluble porous network structures formed by solution self-assembly of opportunely designed building blocks. Since SOFs exhibit their porosity in solution, they are more suitable for applications in drug delivery and energy related fields.

The formation of supramolecular structures and assembled materials is due to molecular self-assembly based on non-covalent interactions. In dissipative self-assembly (DSA), structures and materials are formed far from thermodynamic equilibrium through the constant exchange of energy and matter with the external environment. In fact, in DSA, the formation of the assembled state is not spontaneous, but requires the activation (and deactivation) of the building blocks by a supply of energy, often provided by the addition of chemical fuels.

The ultimate goal of our research project is to develop novel porous supramolecular networks formed from ferrocene-functionalised zinc porphyrins and β-CD dimers (acting as ditopic linker molecules), which can interact thanks to β-CD/ferrocene host-guest interactions. The aim is to exploit the redox-responsive nature of this host-guest interaction to implement DSA in these systems, where the disassembly/assembly of the network can be controlled through the addition of redox chemical fuels. To this aim, we first prepared a novel Fc-functionalised Zn-porphyrin through convergent synthesis and using 'click' chemistry. Then we studied the assembly behaviour in aqueous solution of this porphyrin by UV-Vis and DLS, both alone and in mixture with β-CD or β-CD dimer. In addition, as a comparison, we studied the assembly behaviour of another porphyrin (previously synthesized), bearing longer spacer groups. The results showed that the porphyrin we synthesized self-assembles into larger aggregate structures than the porphyrin with longer spacers, and, in the presence of the β-CD dimer, forms a population of

aggregates with a higher hydrodynamic diameter. However, further studies need to be carried out to determine if this observation can be ascribed to the formation of extended supramolecular networks.

Keywords: Supramolecular Organic Frameworks, dissipative self-assembly, porous supramolecular materials, 'click' chemistry

2. RESUMEN

Los materiales porosos, como los marcos metal-orgánicos (MOF), los marcos covalentes-orgánicos (COF) y los marcos orgánicos supramoleculares (SOF), son de gran interés científico para diversas aplicaciones, como el reconocimiento molecular, la detección, el transporte, la separación y la catálisis. Los MOF y los COF son materiales cristalinos que presentan porosidad en estado sólido, por lo que son insolubles y/o inestables en solución, lo que dificulta sus aplicaciones en medios homogéneos. Por el contrario, los SOF son estructuras de red porosa soluble formadas por autoensamblaje en solución de bloques de construcción oportunamente diseñados. Como muestran su porosidad en solución, son más adecuados para usos como el suministro de fármacos o para aplicaciones relacionadas con la energía.

La formación de estructuras supramoleculares y materiales ensamblados se debe al autoensamblaje molecular basado en interacciones no covalentes. En el autoensamblaje disipativo (DSA), las estructuras y los materiales se forman lejos del equilibrio termodinámico mediante el intercambio constante de energía y materia con el entorno. De hecho, en DSA, la formación del estado ensamblado no es espontánea, sino que requiere la activación (y desactivación) de los bloques de construcción mediante un suministro de energía, a menudo proporcionado por la adición de combustibles químicos.

El objetivo último de nuestro proyecto de investigación es desarrollar nuevas redes supramoleculares porosas formadas a partir de porfirinas de zinc funcionalizadas con ferroceno y dímeros de β-CD (que actúen como moléculas enlazadoras ditópicas), que puedan interactuar β-CD/ferroceno via interacciones host-guest. El objetivo es explotar la naturaleza redox-responsiva de esta interacción host-guest para implementar DSA en estos sistemas, en los que el desmontaje/montaje de la red puede controlarse mediante la adición de combustibles químicos redox. Para ello, en primer lugar, preparamos una nueva porfirina de zinc funcionalizada con Fc mediante síntesis convergente y utilizando química 'click'. A continuación, estudiamos mediante UV-Vis y DLS el comportamiento del ensamblaje en solución acuosa de esta porfirina, tanto sola como en mezcla con β-CD o β-CD dímero. Además, a modo de comparación, estudiamos el comportamiento de ensamblaje de otra porfirina (sintetizada previamente), con grupos espaciadores más largos. Los resultados mostraron que la porfirina que sintetizamos se

autoensambla en agregados más grandes que la porfirina con espaciadores más largos y, en presencia del dímero β-CD, forma una población de agregados con mayor diámetro hidrodinámico. Sin embargo, es necesario realizar más estudios para determinar si esta observación puede atribuirse a la formación de redes supramoleculares extendidas.

Palabras clave: Marcos orgánicos supramoleculares, autoensamblaje disipativo, materiales supramoleculares porosos, química 'click'.

3. INTRODUCTION

3.1. SUPRAMOLECULAR POLYMER NETWORKS

Porous structures are of great interest for applications such as molecular recognition, sensing, transport, separation, and catalysis.[1,2] Among them, porous materials such as Metal-Organic Frameworks (MOFs), formed by coordination interactions between metals and organic linker molecules, and Covalent Organic Frameworks (COFs), formed from organic monomers linked by dynamic covalent bonds, have attracted much scientific interest in the last decade.[2,3] However, MOFs and COFs are crystalline materials (they are porous solids) that typically require harsh conditions for their preparation, and suffer from disadvantages such as poor processability, insolubility and/or instability in solution.[4–6] This makes them less suitable in applications such as homogeneous catalysis or drug delivery.[7]

Therefore, there are increasing attempts in the field of supramolecular chemistry to develop soluble Supramolecular Organic Frameworks (SOFs), which are periodic, porous, and ordered network structures formed by monomers linked through reversible non-covalent interactions. SOFs belong to the larger family of supramolecular polymers, and thus feature dynamic properties in solution along with the possibility to be engineered for stimuli responsiveness. Having access to soluble porous frameworks is an important advantage in drug delivery, biomedical, and energy related applications, when compared with MOFs and COFs.[6,8,9]

Since 2013, several water-soluble 2D and 3D supramolecular frameworks have been synthesised, mainly based on host-guest interactions, and using CB[8] as the host molecule.[7] In 2021, Yang and co-workers demonstrated the formation of a 2D-SOF bilayer based on zinc porphyrins decorated with 4-phenylpyridinium guest subunits, which can dimerize upon encapsulation into the CB[8] host. Axial coordination of ditopic bipyridine ligands to zinc porphyrins laying in two adjacent monolayers enabled the formation of the bilayer.[10]

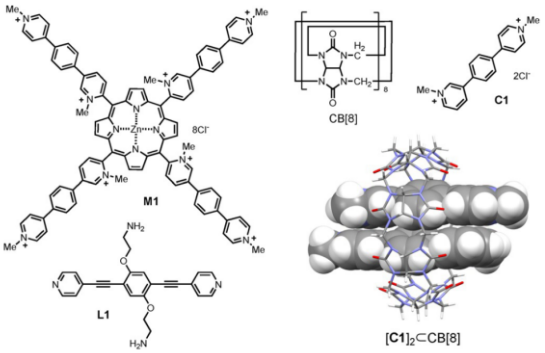

Figure 1: Bilayer 2D-SOF based on zinc porphyrins and CB[8]. Adapted from ref. 10.

The 2D SOF formed by porphyrins are ordered periodic assemblies of chromophores, and thus they are useful models for studying phenomena such as light harvesting, aggregation-induced emission and energy transfer.[10–12]

3.2. DISSIPATIVE SELF – ASSEMBLY

The formation of supramolecular structures and self-assembled functional materials is due to molecular self-assembly based on non-covalent interactions. There are two types of artificial self-assembly. In the most common, artificial materials are synthesised under equilibrium conditions, through spontaneous processes that are governed by thermodynamic stability and do not require an external energy source or fuels to proceed. On the other hand, in dissipative self-assembly (DSA), structures and materials are formed far from thermodynamic equilibrium through the constant exchange of energy and matter with the external environment.[13–15]

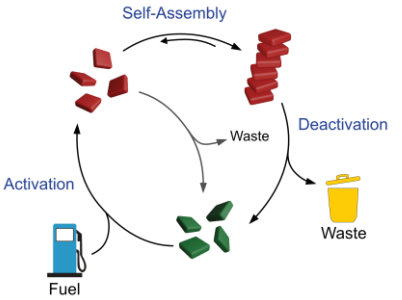

Figure 2: Schematic representation of dissipative self-assembly.

In DSA the formation of the assembled state is not spontaneous but requires the activation of the building blocks using an energy supply, for example provided by addition of a chemical fuel. In addition, deactivation of the building blocks to return the system to the non-assembled state is also required, which may or may not use a chemical fuel. Therefore, in DSA, the self-assembly is not governed by the relative stability of the assembled and disassembled states, as it occurs under thermodynamic control, but rather the assembly depends on the kinetics of the fuel-to-waste conversion cycle.[14,15] Artificial DSA is inspired by living systems, which use chemical fuels to achieve spatio-temporal control over the structures and functions of important supramolecular assemblies such as the actin filaments in the cell cytoskeleton.

So far, several chemical fuel-driven artificial self-assembled systems have been developed, such as colloids,[16] supramolecular gels,[17] vesicles[18] and supramolecular polymers,[19] but still DSA has not been demonstrated for supramolecular polymer networks.

3.3. HOST – GUEST INTERACTIONS

Non-covalent reversible interactions such as H-bonding, π-π stacking, electrostatic interactions, Van Der Waals forces and host-guest interactions are used for the formation of discrete supramolecular structure and supramolecular polymers.[1]

Host-guest interactions have been largely used for the formation of self-assembled hierarchical structures.[20,21] These interactions occur between two or more molecules that have a specific structural relationship, where the larger 'host' molecule (typically a macrocycle) recognises and reversibly binds one or more smaller 'guest' molecules, resulting in a host-guest complex. By exploiting the reversibility of the host-guest interactions, supramolecular systems that can be assembled or disassembled in response to external stimuli such as light, redox stimuli, pH, and temperature variations have been prepared.[22]

A widely exploited host-guest interaction in supramolecular chemistry is that formed by the 'host' β-cyclodextrin (β-CD), a cyclic heptamer of glucose, and the 'guest' ferrocene (Fc). This interaction is redox responsive, where the ferrocene only binds to the hydrophobic cavity of β-CD when it is in its neutral (reduced) form, yielding a 1:1 complex with a high association constant. In contrast, the complex dissociates when Fc is oxidised to the more hydrophilic ferrocenium ion (Fc^+).[23] This property has been used to synthesise redox-responsive supramolecular and

polymeric systems, such as self-healing hydrogels, and redox-sensitive drug delivery systems.[22,24,20]

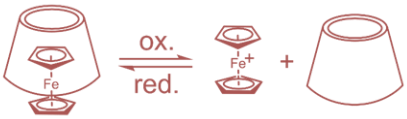

Figure 3: Redox-responsive β-CD/Fc host-guest interaction.

3.4. OUR SYSTEM

The final goal of the research project, of which this TFG work is a part, is to develop novel porous supramolecular polymer networks formed from two main components: i) Fc-functionalized zinc porphyrins; and ii) β-CD dimers acting as ditopic linker molecules. The aim is to exploit the redox-responsive nature of the β-CD/Fc host-guest interactions to control the disassembly/reassembly of the network, via the addition of oxidant and reductant chemical fuels (Figure 4). We envision that dissipative self-assembly can be achieved in these systems, for example by modulating the supply of the chemical fuels into a solution of the building blocks, to control the lifetime of the assembled state.

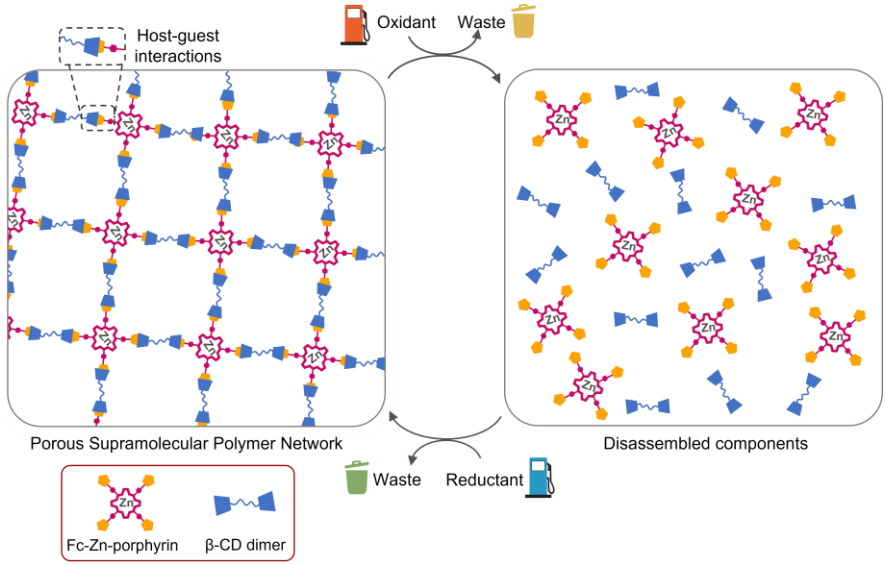

Figure 4: Chemically fueled dissipative self-assembly of a supramolecular polymer network based on β-CD/Fc host-guest interactions.

In a previous TFG project,[25] a symmetric Zn-tetraphenylporphyrin tethered to four ferrocene moieties through a tetraethylene glycol (TEG) spacer was synthesized (**P4**), to be used as a building unit in such supramolecular systems together with a β-CD dimer (Figure 5). The TEG chains were included in the design of **P4** to enhance its water solubility and yield larger pore sizes in the assembled network, while the central metal can be used as acceptor site for axial coordination, for example enabling the formation of bilayered hierarchical structures in the presence of bidentate ligands.[10] However, only very preliminary assembly studies were performed with this porphyrin.

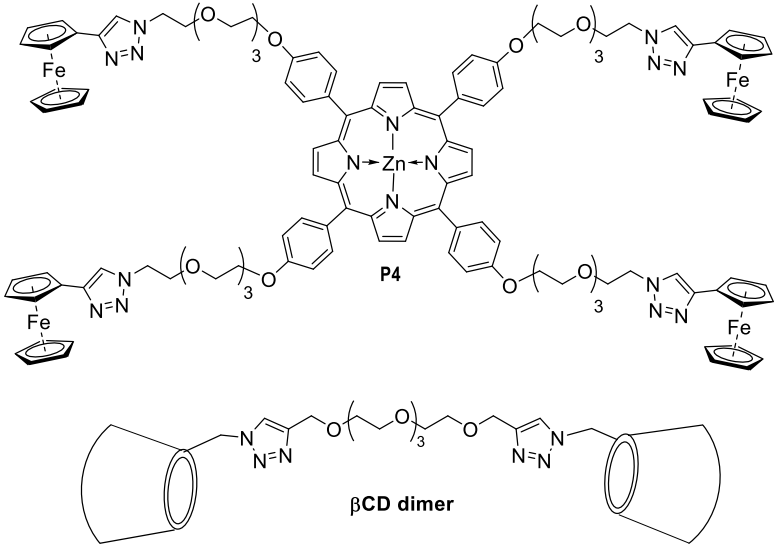

Figure 5: Chemical structure of **P4** and β-CD dimer.

4. OBJECTIVES

In this TFG work we aim to perform more extensive studies into the assembly behaviour of the previously synthesised porphyrin **P4**, whilst also preparing a novel Zn-porphyrin, featuring a shorter spacer between the porphyrin unit and the peripheral ferrocene moieties (**P6**), to compare the assembly behaviour of the two systems. We foresee that removing the long and flexible TEG fragments will lower the porphyrin aqueous solubility (higher hydrophobicity), potentially enhancing its interaction with the β-CD dimer due to solubilization effects, while providing a more rigid network structure with smaller pores. The specific objectives of this TFG were:

- Synthesis and characterization of a novel Fc-functionalized Zn-porphyrin (**P6**), as building unit for supramolecular polymer networks.
- Studying and comparing the assembly behaviour of **P4** and **P6** in aqueous media both alone and in the presence of β-CD or β-CD dimer (UV-Vis and Dynamic Light Scattering).

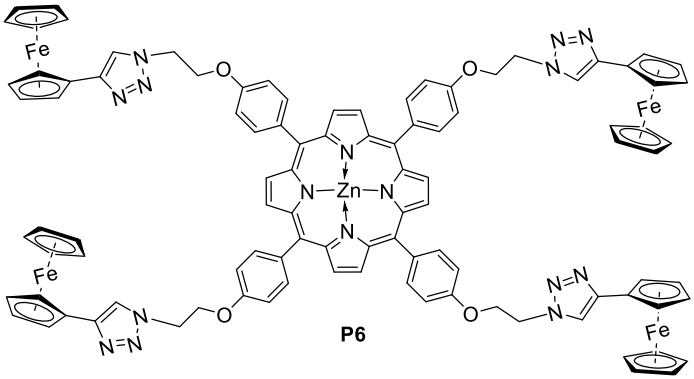

Figure 6: Structure of the target porphyrin **P6**.

5. RESULTS AND DISCUSSION

5.1. SYNTHESIS OF PORPHYRIN P6

With the aim of building a 2D supramolecular network based on host-guest interactions, a new symmetric Zn-tetraphenylporphyrin bearing four ferrocene (guest) moieties at its periphery, linked through an ethylene-triazole spacer, has been designed and prepared (**P6**). The retrosynthetic analysis for the preparation of **P6** is shown in Scheme 1.

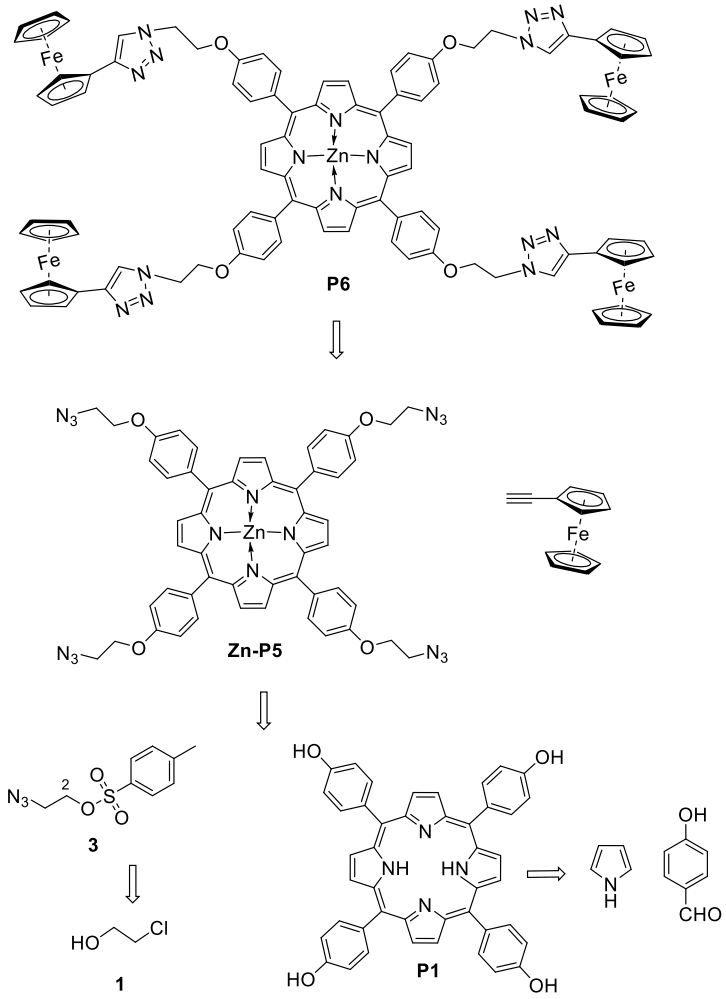

Scheme 1. Retrosynthetic analysis for the preparation of porphyrin **P6**.

The Fc-functionalized porphyrin **P6** was synthesised via 'click' chemistry starting from the tetra-azide Zn-porphyrin **Zn-P5** and ethynyl ferrocene (commercially available), by using copper catalysed azide-alkyne cycloaddition (CuAAC). The porphyrin **Zn-P5** was obtained by metalation of the corresponding free-base porphyrin **P5**, which in turn was obtained by convergent synthesis, combining compound **3** with the 5,10,15,20-Tetrakis(4-hydroxyphenyl)porphyrin **P1** via Williamson type *O*-alkylation. Compound **3** was synthesized in two-steps starting from commercially available 2-chloroethanol, while porphyrin **P1** was prepared by condensation of pyrrole with 4-hydroxybenzaldehyde.

The ethylene linker, much shorter than the TEG linker introduced in the previously synthesised porphyrin **P4**, was introduced in the design of **P6** with the aim of having a more compact supramolecular network, and with smaller size of the lattice pores, as compared to **P4**.

The binding of the ferrocene by a 'click' reaction was performed after obtaining the porphyrin **Zn-P5**, and not on compound **3**, as this intermediate tetra-azide porphyrin can be a valuable scaffold for other projects running in the lab, such as the conjugation to biopolymers.

5.1.1. Synthesis of porphyrin P1

Porphyrin **P1** was synthesised as shown in Scheme 2, according to a previously reported procedure.[26,27]

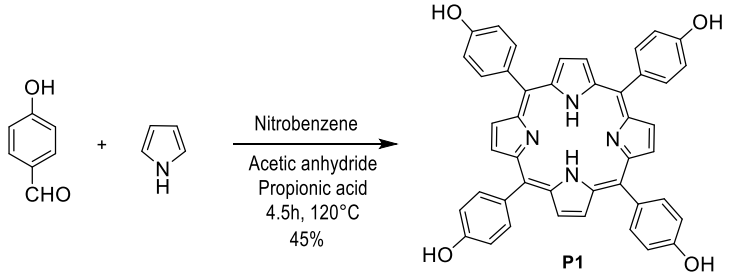

Scheme 2. Synthesis of porphyrin **P1**.

Specifically, we used a modified version of the Adler-Longo method, in which the condensation reaction between 4-hydroxybenzaldehyde and pyrrole is carried out in a mixture propionic acid, acetic acid, and nitrobenzene (3:1:2), with the latter playing both the role of co-solvent as well as of oxidant for the intermediate porphyrinogen. Following this protocol, a solution of pyrrole in nitrobenzene and 4-hydroxybenzaldehyde in propionic acid were added dropwise,

and simultaneously, to a refluxing mixture of the three solvents. After additional 1.5 h at reflux, the heating was stopped, and air was bubbled into the reaction mixture to facilitate the complete oxidation. Afterwards, hexane was added, and mixture was left in the fridge to induce the precipitation of the crude product as a black powder, which was purified by solid-liquid extractions using a Soxhlet apparatus and ethyl acetate as the solvent.

We attempted to synthesize **P1** two times by following this protocol, however, we could only obtain the product in very low yields after purification (< 2%) (see *Protocol 1* in the Experimental Section). The first time, we ascribed the low yield to the fact that the addition rate of the reactants was not well commensurate, so that the addition of pyrrole was completed much sooner than that of the aldehyde. Unfortunately, however, even when we repeated the reaction by carefully following the reported procedure, we could not obtain a significant improvement of the yield, mainly due to a very low extent of precipitation from hexane (even when using an excess of this solvent). In addition, the UV-Vis spectrum of the crude revealed only a small band ascribable to the Soret band of the porphyrin against a broad absorption background (Appendix 1). Furthermore, liquid chromatography-mass spectrometry (LC-MS) analysis of the crude revealed the presence of a main subproduct (along with the target product **P1**, and various other oligomeric species) with mass $[M + 1]^+ = 237.1$ and a broad absorption band centred at 467 nm, which we could identify as the 5-(4-hydroxyphenyl)dipyrromethene.

We therefore decided to repeat the reaction by using slightly modified conditions for the reaction, the workup, and the purification (see *Protocol 2* in the Experimental Section). Namely, we: (i) reduced the fraction of nitrobenzene (from 32 to 22%); (ii) worked in more concentrated conditions to favour the following precipitation (70 mM instead of 30 mM); (iii) increased the reaction time to 4.5 h (while monitoring the reaction progress by UV-Vis); (iv) added the hexane to the reaction mixture and not vice versa; (v) used methanol as the extraction solvent. The UV-Vis of the reaction mixture at 4 h showed an intense Soret Band and four detectable Q-bands, together with a shoulder at 465 nm that completely disappeared in the purified product after Soxhlet extractions (Appendix 1). By using this optimized procedure, **P1** was obtained as a blue crystalline solid with a 45% yield, which was characterized by ^{1}H NMR and mass spectrometry (see Experimental Section).

5.1.2. Synthesis of compound 3

The synthetic route to prepare compound **3** is described in Scheme 3.

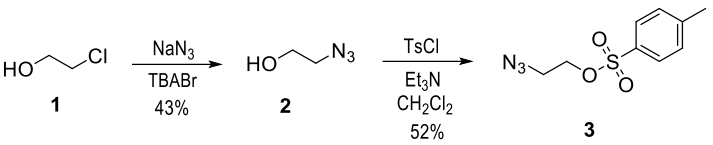

Scheme 3. Synthesis of compound **3**.

The first step was the preparation of the 2-azidoethanol **2**, starting from commercially available 2-chloroethanol **1**, which was refluxed in the presence of sodium azide and tetrabutylammonium bromide as the catalyst. The reaction was carried out using an excess of sodium azide, according to a previously reported procedure,[28] and was run behind a safety shield. This functional group interconversion (FGI) is a nucleophilic substitution (S_N2 reaction), in which the good leaving group chlorine is substituted by the azide group (nucleophile). Purification of compound **2** was achieved by distillation. In the second step, tosylation of 2-azidoethanol **2** with *p*-toluenesulfonyl chloride in DCM, in the presence of triethylamine, afforded the orthogonally functionalized compound **3**, which was purified by column chromatography on silica gel. Compounds **2** and **3** (yellowish oils) were characterised by ^{1}H NMR to confirm their identity and purity (see Experimental section).

5.1.3. Synthesis of porphyrin P6

Having prepared the core porphyrin **P1** and the linker **3**, the next step was the preparation of the target porphyrin **P6**, following the three-step synthetic route shown in Scheme 4.

Firstly, we prepared the free-base tetra-azide porphyrin **P5** via *O*-alkylation of the phenol groups of **P1** with compound **3** in the presence of potassium carbonate as base, and potassium iodide as catalyst (Williamson etherification).[29] The reaction was carried out in DMF at 80ºC for 8 days, while its progress was monitored by LC-MS, showing the gradual appearance of the mono-, bis-, tris- and tetra- alkylated products. However, to our surprise, from the fourth day a secondary series of peaks started to appear in the LC-MS chromatogram, corresponding to porphyrin products (as confirmed by their UV-Vis absorption) with the mass of the partially alkylated species (mono-, bis-, tris- and tetra-) plus 126. These species correspond to monoiodinated products. It has been reported that tetrahydroxyphenyl porphyrins, bearing phenol groups that are very reactive to electrophilic aromatic substitution, can be monoiodinated (in their *ortho*- position) with

iodide salts in the presence of oxidants that form electrophilic iodine species (e.g., H_2OI^+ or hypoiodous acid).[30,31]

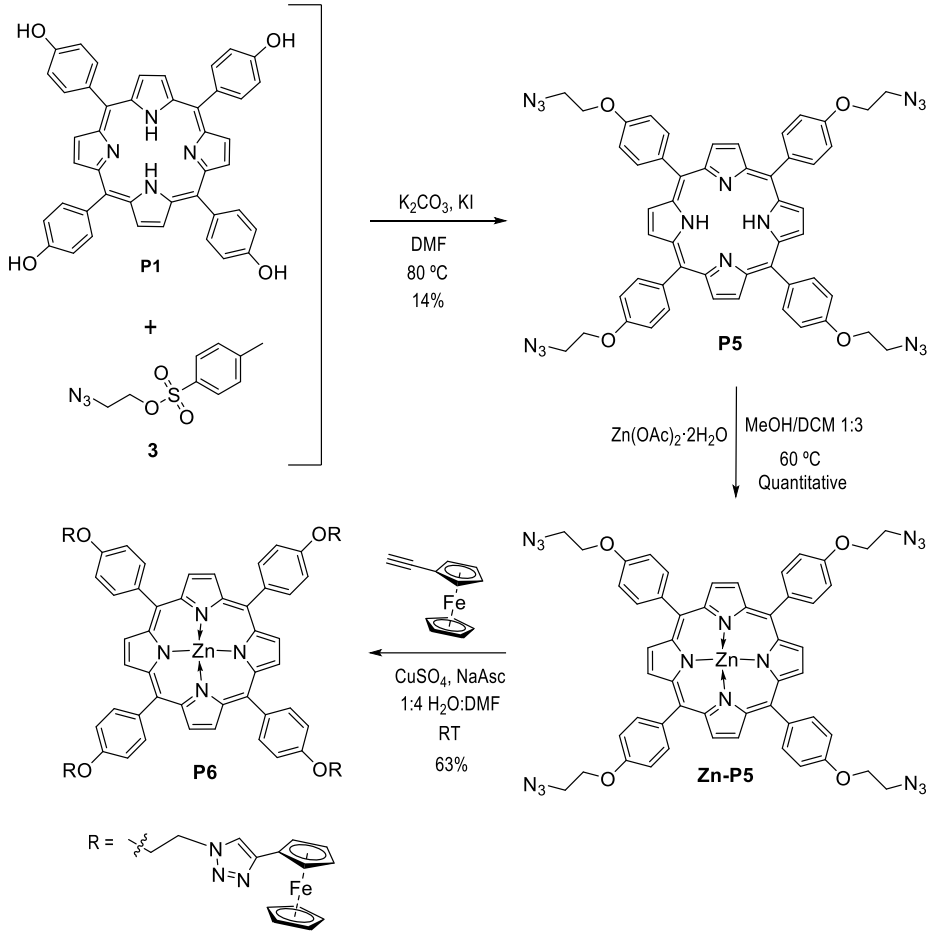

Scheme 4. Synthesis of the target porphyrin **P6.**

Our hypothesis is that, under prolonged harsh reaction conditions, and since the reaction was performed under air, oxidation of iodine may have occurred, explaining the experimental outcome. In addition, some photooxidation processes, facilitated by the porphyrin chromophores, may have happened, since the reaction was not performed in darkness. After 8 days, since the alkylation was not going to completion, even after adding more compound **3** (4 equivalents), we decided to stop the reaction and perform a purification by column chromatography on silica gel, which allowed us to isolate a mixture of the tris- (most abundant) and tetra- alkylated products. This

mixture was put to react again with **3** under the same reaction conditions as before, but without using potassium iodide, resulting in the complete formation of the tetraalkylated product **P5**, which was purified by column chromatography using hexane/ethyl acetate gradient as mobile phase (see Experimental Section). Eventually, **P5** was obtained as a pink-purple solid (14% yield).

The next step was the metalation of the free-base porphyrin **P5** using zinc acetate dihydrate in a 1:3 MeOH/DCM solvent mixture at reflux. The progress of the reaction was easily monitored by UV-Vis, since the free-base porphyrin is characterized by four Q-bands, while the metalated porphyrin has two Q-bands due to its higher symmetry. After workup, the Zn-porphyrin, **Zn-P5**, was obtained as a pink solid in quantitative yield, that was used in the next step without further purification (see Experimental Section).

Finally, porphyrin **P6** was prepared from **Zn-P5** and ethynyl ferrocene via 'click' chemistry in a DMF/water solvent mixture. The reaction is a Huisgen-type copper-catalysed [3+2] azide-alkyne cycloaddition (CuAAC), resulting in the formation of a stable five-membered triazole ring. The Cu(I) catalyst was generated in situ by reduction of $CuSO_4$ with sodium ascorbate. The progress of the reaction was monitored by LC-MS until only the tetra-ferrocene product **P6** was observed. As the reaction proceeded, a purple solid started to precipitate from the reaction mixture. The workup and purification consisted in separating this purple solid by centrifugation, followed by repeated washes with DMF and methanol (using centrifugation before solvent decantation), which allowed us to completely remove the unreacted ethynyl ferrocene, affording pure **P6** as a purple solid (63% yield). The final compound was characterised by IR (which confirmed the absence or the characteristic azide band), ^{1}H NMR, ^{13}C NMR and mass spectrometry (see Experimental Section). Remarkably, compound **P6** was found to be highly insoluble in all the solvents we tested, including DMF, DMSO, MeOH, acetonitrile, THF and chlorinated solvents. However, it could be readily solubilized (e.g., in acetonitrile and THF) by addition of pyridine, most likely due to the coordination of the pyridine to the Zn metal centre.

5.2. UV-Vis and DLS studies

As the first step towards the final goal of obtaining supramolecular polymer networks based on Fc-functionalised porphyrins **P4** (bearing a long TEG spacer) and its shorter analogue **P6**, and driven by Fc-CD host/guest interactions, we studied the solution behaviour of **P4** and **P6** alone, and in mixtures with β-CD or β-CD dimer by UV-Vis spectroscopy and Dynamic Light Scattering

(DLS). The studied samples (aqueous solutions) were prepared by using a co-solvent approach according to the protocols detailed in the Experimental Section.

5.2.1. Studies with porphyrin P4

The UV-Vis spectrum of porphyrin **P4** in THF shows a sharp Soret band at 426 nm together with two Q-bands at 557 and 598 nm, which indicates the presence of molecularly dispersed Zn-porphyrin in solution. The intensity of the absorption spectrum increases linearly with the concentration of **P4** (in the concentration range 0.5 – 5 μM), according to the Lambert-Beer Law (Figure 7A), from which we could calculate the molar extinction coefficient of **P4** in THF at 426 nm (ε_{426} = 514100 ± 2850 M^{-1} cm^{-1}) (inset in Figure 7A).

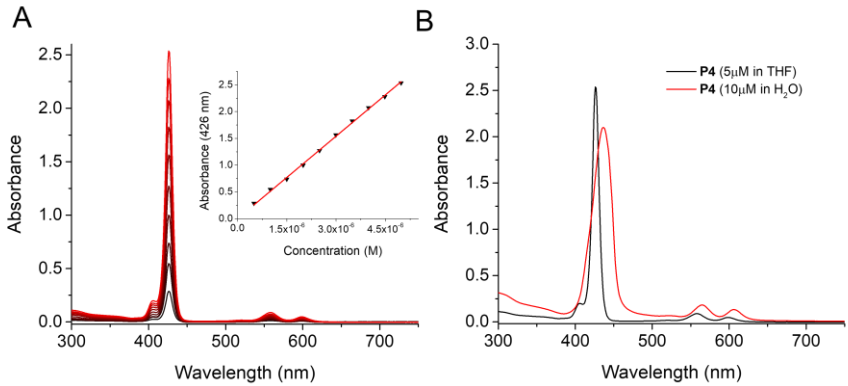

Figure 7. A) UV-Vis spectra of **P4** in THF at different concentrations. Inset: absorbance at 426 nm versus concentration and linear fitting; B) UV-Vis spectra of **P4** in THF (5 μM) and water (10 μM). L = 1 cm.

As expected, DLS measurements confirmed the absence of aggregate species (zero scattering intensity). In striking contrast, solutions of **P4** in water (at 10 μM) show red-shifted Soret and Q-bands (> 10 nm), with an evident broadening and decrease in intensity (hypochromicity) of the former (red line in Figure 7B). This suggests the formation of aggregate species in solution (inter-chromophore interactions) formed by self-assembly of **P4**. DLS measurements confirmed the presence of a rather homogeneous population of scatterers with an average hydrodynamic diameter of 92 nm (Table 1) and polydispersity index PDI = 0.136 (raw DLS data showing the goodness of fit of the Cumulant analysis are reported in Appendix 3).

	1h			24 h		
	P4 (10 µM)	**P4+ βCD** (10 / 20 µM)	**P4+ βCD** (10 / 40 µM)	**P4** (10 µM)	**P4+ βCD** (10 / 20 µM)	**P4+ βCD** (10 / 40 µM)
Z-average [nm]	92.2	119.5	76.0	91.8	118.2	76.3
PDI	0.136	0.148	0.150	0.115	0.111	0.126

Table 1: Results from the DLS measurements of samples of **P4**.

Interestingly, the spectrum of **P4** (10 µM) in the presence of 20 µM β-CD (β-CD/Fc host-guest ratio 0.5 :1) exhibits further broadening and red-shift of the Soret band (blue line in Figure 8A), which corresponds to an increase of the average size of the aggregates to 120 nm, as assessed by DLS (Table 1). On the other hand, increasing the concentration of β-CD to 40 µM (β-CD/Fc host-guest ratio 1:1) resulted in a sharpening and blue-shift of the Soret band, along with a decrease of the average size of the aggregates down to 76 nm. These changes likely suggest the occurrence of β-CD/Fc host-guest interactions that perturb the structure of the self-assemblies of **P4**.

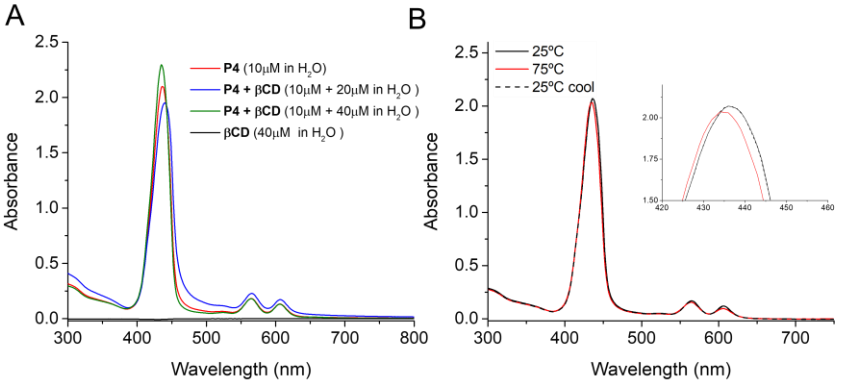

Figure 8. A) UV-Vis spectra of **P4** in water (10 µM) alone and in the presence of different concentrations of β-CD; B) UV-Vis spectra of **P4** in water (10 µM) at different temperatures. L = 1 cm

The UV-Vis and DLS measurements were repeated on the same samples after 24 h and 48 h, giving almost identical results (Table 1), indicating that neither ageing of the aggregates, nor precipitation take place.

Additionally, we performed temperature scan experiments for all the investigated samples, in which the UV-Vis spectra were recorded every 5 ºC from 25 to 75 ºC (and again at 25 ºC upon cooling), and DLS was measured before and after the heating/cooling cycle. To our surprise, only

tiny reversible changes were observed in the UV-Vis spectra of **P4** both in the absence of β-CD (Figure 8B), and in the presence of β-CD (Appendix 2). Additionally, no variation in the size of the aggregates were detected by DLS. Overall, these results suggest a very strong thermodynamic (or kinetic) stability of the assemblies formed by **P4**. Further studies (Fluorescence spectroscopy, AFM) need to be carried out to assess the exact structure and morphology of these species.

5.2.2. Studies with porphyrin P6

With the new synthesised porphyrins **P6** at a hand, we performed preliminary studies of its assembly behaviour in water (at 10 μM), both alone and in the presence of β-CD (40 μM and 200 μM) and β-CD dimer (20 μM and 100 μM) by UV-Vis and DLS measurements. As in the case of **P4**, the spectrum of **P6** in water shows a broad Soret band, even less intense than in **P4** (Figure 9A), which corresponds to aggregates with an average hydrodynamic diameter of 170 nm (Table 2), i.e. double the size of those formed by **P4** at the same concentration conditions.

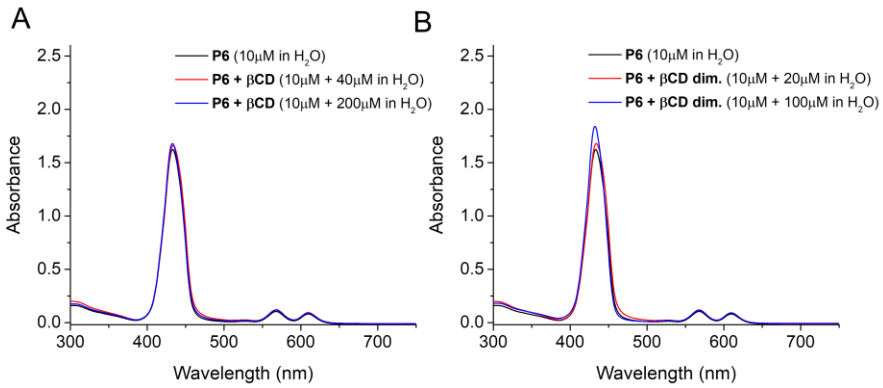

Figure 9. A) UV-Vis spectra of **P6** in water (10 μM) alone and in the presence of different concentrations of β-CD; B) UV-Vis spectra of **P6** in water (10 μM) alone and in the presence of different concentrations of β-CD dimer. L = 1 cm

This is not surprising, considering that the absence of the 'solubilizing' TEG moieties should render **P6** more prone to assemble in water. Contrarily to the case of **P4**, the presence of β-CD up to 200 μM (i.e., β-CD/Fc host-guest ratio 5 :1) barely affects the UV-Vis spectrum of **P6** (Figure 9A), while promoting an increase of the size of the aggregates up to 230 nm as shown in Table 2. This suggests that the inter-chromophore interactions are not perturbed by potential host-guest

interactions occurring between the β-CD and the Fc moieties (e.g., because they may happen only at the surface of the assemblies).

	P6 (10 μM)	**P6+ βCD** (10 / 40 μM)	**P6+ βCD** (10 / 200 μM)	**P6+ βCD dimer** (10 / 20 μM)	**P6+ βCD dimer** (10 / 100 μM)
Z-average [nm]	171.3	202.3	231.0	200	195* (150 / 500)
PDI	0.130	0.164	0.196	0.145	0.255

Table 2: Results from the DLS measurements of samples of **P6**.

On the other hand, the presence of the β-CD dimer at 100 μM (i.e., β-CD/Fc host-guest ratio 5:1) promotes a sharpening and increase of intensity of the Soret band (blue line in Figure 9B), which is accompanied by an 'apparent' decrease in size of the assemblies (Table 2). It must be stressed, in fact, that in this case the DLS data could not be properly fit by only assuming a single monomodal population (by Cumulant analysis), as we did for all the other samples, but we instead had to consider two different populations of scatterers (multimodal distribution centred at around 150 and 500 nm) to achieve a good fitting (see Appendix 4). Further studies (AFM, Small Angle X-Ray Scattering) need to be carried out to assess if the observation of a population with higher hydrodynamic diameter can correspond to the formation of extended supramolecular networks, with reduced interchromophore interactions explaining the sharpening of the Soret band.

6. EXPERIMENTAL SECTION

6.1. MATERIALS AND METHODS

Sodium azide, 2-chloroethanol, tetrabutylammonium bromide, *tert*-butyl methyl ether, triethylamine, *p*-toluenesulfonyl chloride, dichloromethane, magnesium sulfate, propionic acid, nitrobenzene, glacial acetic acid, 4-hydroxybenzaldehyde, hexane, ethyl acetate, dimethylformamide, potassium carbonate, methanol, zinc acetate dihydrate, coppper sulfate, sodium ascorbate, ethynyl ferrocene, tetrahydrofuran, dimethyl sulfoxide-d6, chloroform-d, and pyridine-d5 were obtained from commercial suppliers and used as received, with the exception of pyrrole, which was distilled under reduced pressure shortly before use.

β-cyclodextrin dimer (β-CD dimer) as well as **P4** were previously synthesized in the group.

Thin-layer chromatography (TLC) of all products and crude reaction mixtures were performed on aluminium plates coated with a 0.2 μm layer of silica gel (60 F, 245 nm, Merck). TLC results were visualized directly under a UV lamp or upon vanillin staining.

Flash column chromatography was performed using silica gel 60 A° (35-70 μm) from Acros Organics.

NMR spectra were recorded at 25 °C on Bruker 400 MHz or Bruker 500 MHz spectrometers. $CDCl_3$, d6-DMSO, and pyridine-d5 were used as solvents. Coupling constants (J) are given in Hz and peak multiplicities are specified as following: s, singlet; d, doublet; t, triplet; m, multiplet; dd, doublet of doublets; dt, doublet of triplets.

Mass spectra (electrospray ionization, ESI-MS) were obtained using a HPLC Waters 2695 equipped with a Micromass ZQ quadrupole analyzer.

UV-Vis spectra were recorded using an Agilent Cary 60 spectrophotometer equipped with a Peltier heating/cooling accessory.

DLS measurements were performed with a VASCO Kin DLS system from Cordouan Technologies at room temperature (laser wavelength 638 nm).

6.2. SYNTHESIS OF PORPHYRIN P6

6.2.1. Synthesis of 2-azidoethanol, 2

Sodium azide (5.096 g, 78.4 mmol, 1.73 eq.), 2-chloroethanol (3.643 g, 45.3 mmol, 1.0 eq.) and tetrabutylammonium bromide (0.836 g, 2.60 mmol, 0.06 eq.) were mixed and stirred at 110 ºC over 18 hours with a safety shield. The resulting oil was diluted with *tert*-butyl methyl ether and unreacted solid removed by filtration. The solvent was evaporated under reduced pressure without heating, yielding a yellow oil. The crude product was purified by distillation under reduced pressure and the pure product obtained as a colourless oil (1.674 g, 43% yield).

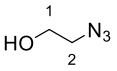

2

^{1}H NMR (500 MHz, $CDCl_3$) δ (ppm): 3.78 (t, J = 5.7 Hz, 2H, H_1), 3.45 (t, J = 5 Hz, 2H, H_2), 2.18 (t, J = 5.8 Hz, 1H, -OH).

6.2.2. Synthesis of 2-azidoethyl-4-methylbenzenesulfonate, 3

2-azidoethanol (1.5 g, 17.2 mmol, 1.0 eq.) and Et_3N (2.61 g, 25.8 mmol, 1.5 eq.) were added to DCM (88 mL) under stirring. Afterwards, *p*-toluenesulfonyl chloride (4.918 g, 25.8 mmol, 1.5 eq.) was added and the mixture was stirred for 18 h at room temperature under nitrogen. Then, the reaction was quenched by addition of water (90 mL), the layers separated, and the aqueous phase was extracted with DCM (2 x 100 mL). The combined organic phase was dried over $MgSO_4$ and the solvent was removed under reduced pressure to obtain a yellow oil. The crude product was purified by column chromatography (silica gel, 100% DCM) yielding the pure compound **3** as a pale yellow oil (2.151 g, 52% yield).

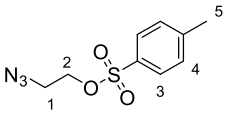

3

^{1}H NMR (500 MHz, $CDCl_3$) δ (ppm): 7.83 (d, J = 8 Hz, 2H, H_3), 7.36 (d, J = 8 Hz, 2H, H_4), 4.16 (t, J = 5.2 Hz, 2H, H_1), 3.49 (t, J = 5.2 Hz, 2H, H_2), 2.46 (s, 3H, H_5).

6.2.3. Synthesis of 5, 10, 15, 20-tetrakis(4-hydroxyphenyl)porphyrin, P1

Protocol 1: Propionic acid (50 mL), nitrobenzene (25 mL) and glacial acetic acid (25 mL) were mixed in a 250 mL three-neck round-bottom flask (r.b.f.) and heated at 120 ºC for 30 min. Then, a solution of 4-hydroxybenzaldehyde (0.555 g, 4.54 mmol, 1.0 eq.) in propionic acid (30 mL) and a solution of pyrrole (0.306 g, 4.56 mmol, 1.0 eq.) in nitrobenzene (25 mL), were added to the reaction mixture dropwise at the same time, and the mixture was then refluxed for 1.5 h. The mixture was cooled to room temperature, and then air was blown into it for 30 min. Afterwards, the reaction mixture was poured into hexane (60 mL) and left into the fridge over 48 h to precipitate a small amount of a black solid which was collected by filtration, washed with hexane, and dried. The crude product was purified by solid-liquid extractions using a Soxhlet extractor and ethyl acetate as the solvent (250 mL). The solvent was removed under reduced pressure and **P1** was obtained as a dark blue solid (< 2% yield).

Protocol 2: A mixture of propionic acid (30 mL), glacial acetic acid (20 mL) and nitrobenzene (10 mL) were heated at reflux (125 ºC) for 30 min in a three-neck r.b.f. Then, a solution of 4-hydroxybenzaldehyde (0.672 g, 6.00 mmol, 1.0 eq.) in propionic acid (15 mL) and a solution of pyrrole (0.402 g, 6.00 mmol, 1.0 eq.) in nitrobenzene (10 mL), were added to the solvent mixture dropwise and simultaneously over 10 min. After a few minutes, the reaction mixture turned deep black. The progress of the reaction was monitored by UV-Vis (dissolving an aliquot of the crude in methanol) revealing the progressive appearance of an intense Soret band at 419 nm. After 4.5 h at reflux, the reaction mixture was cooled to room temperature and air was blown into it for 30 min. Then hexane (100 mL) was added directly into the three-neck r.b.f., and the resulting mixture was left in the fridge (4ºC) for two days, and cooled additionally for 2 h at 0ºC, resulting in the precipitation of the crude product, as a fine black powder. The suspension was filtered on a Gooch funnel (nº 4) and the precipitate was washed with hexane. In addition, the large amount of sticky black tar which remained on the flask walls was first washed with hexane, and then extracted several times with methanol (yielding red solutions), until no further colour could be extracted. The joined methanolic extracts were evaporated under reduced pressure yielding a blue crystalline solid. This solid was merged with the filtered precipitate and subjected to solid-liquid extractions in a Soxhlet apparatus using methanol as the solvent (150 mL), which eventually afforded pure compound **P1** as a brilliant blue solid (0.461 g, 45% yield).

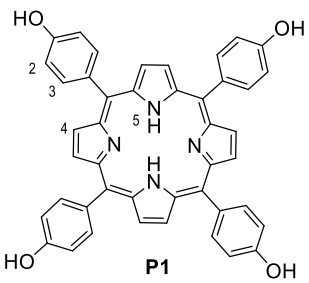

P1

^{1}H NMR (500 MHz, DMSO-d_6) δ (ppm): 8.87 (s, 8H, H_4), 8.00 (d, *J* = 8.3 Hz, 8H, H_2), 7.21 (d, *J* = 8.3 Hz, 8H, H_3), -2.88 (s, 2H, H_5); MS (ESI): m/z calcd. For $C_{44}H_{30}N_4O_4$ = 678.23, found $[M + H]^+$ = 679.52.

6.2.4. Synthesis of P5

Compound **3** (1.045 g, 4.33 mmol, 8.0 eq.) and K_2CO_3 (1.004 g, 7.26 mmol, 14 eq.) were added to a solution of porphyrin **P1** (0.350 g, 0.515 mmol, 1.0 eq.) in DMF (10 mL). The mixture was stirred at 80 ºC for 8 days, with the progress of the reaction monitored by LC-MS. Afterwards, most of the DMF solvent was removed under reduced pressure, water was added, and the aqueous phase was extracted with DCM (3 x 20 mL). The combined organic phases were washed with brine, dried with $MgSO_4$ and filtered, and the solvent was removed under reduced pressure. The crude product was purified by column chromatography (silica gel, 5:5 hexane/ethyl acetate to ethyl acetate and methanol). The pure product was obtained as a violet solid **P5** (0.0698 g, 14% yield).

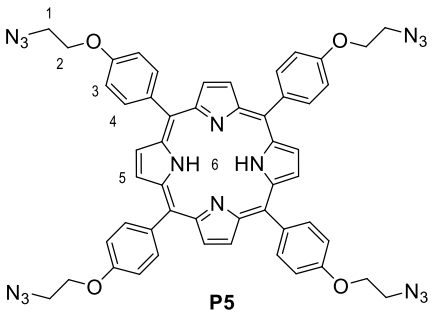

P5

^{1}H NMR (500 MHz, $CDCl_3$) δ (ppm): 8.86 (s, 8H, H_5), 8.13 (d, *J* = 8.0 Hz, 8H, H_3), 7.31 (d, *J* = 8.0 Hz, 8H, H_4), 4.46 (t, *J* = 4.0 Hz, 8H, H_2), 3.80 (t, *J* = 4.0 Hz, 8H, H_1). UV-Vis (MeOH) λ_{max}, nm = 421 (Soret), 518, 555, 596, 651 (Q bands). MS (ESI): m/z calcd. For $C_{52}H_{42}N_{16}O_4$ = 954.36, found $[M + H]^+$ = 955.3.

6.2.5. Synthesis of Zn-porphyrin, Zn-P5

A solution of $Zn(OAc)_2 \cdot 2H_2O$ (0.056 g, 0.305 mmol, 4.0 eq.) in MeOH (10 mL) was added to a solution of compound **P5** (0.0597 g, 0.0626 mmol, 1.0 eq.) in DCM (30 mL), the mixture was stirred at 60 ºC under nitrogen overnight. The completion of the reaction was verified by UV-Vis, by disappearance of the four Q-bands of the free base porphyrin and appearance of two new Q-bands for the metalated compound. Then, the reaction mixture was cooled to room temperature and more DCM (40 mL) was added. The organic phase was washed with H_2O (2 x 40 mL), dried over $MgSO_4$, and filtered. After removal of the solvent under reduced pressure, **Zn-P5** was obtained as a purple solid (0.0612 g, 96% yield), and directly used in the next step without further purification.

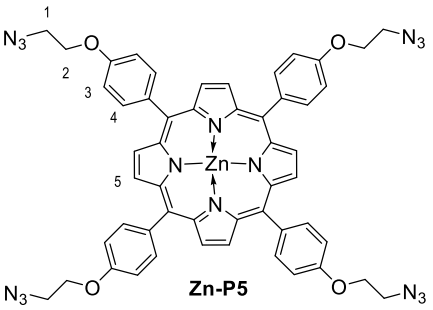

Zn-P5

UV-Vis (DCM): λ_{max} ,nm = 425 (Soret), 555, 595 (Q-bands).

6.2.6. Synthesis of target porphyrin, P6

To a solution of compound **Zn-P5** (0.0612 g, 0.0601 mmol, 1.0 eq.) in 6 mL of H_2O/DMF (1:4), ethynyl ferrocene (0.0594 g, 0.283 mmol, 5 eq.), $CuSO_4$ (0.008 g, 0.0501 mmol, 0.8 eq.) and sodium ascorbate (0.0279 g, 0.141 mmol, 2 eq.) were added. The reaction mixture was stirred over 3 days under nitrogen at room temperature (the progress of the reaction was monitored by LC-MS). As the reaction proceeded, a purple solid precipitated out of the reaction mixture. The solid was separated by centrifugation and washed with further DMF (2 x 10 mL) and MeOH (3 x 10 mL), where the methanol washes allowed the complete removal of the unreacted ethynyl ferrocene in excess. This afforded the pure compound **P6** (0.0703 g, 63% yield) as a purple solid.

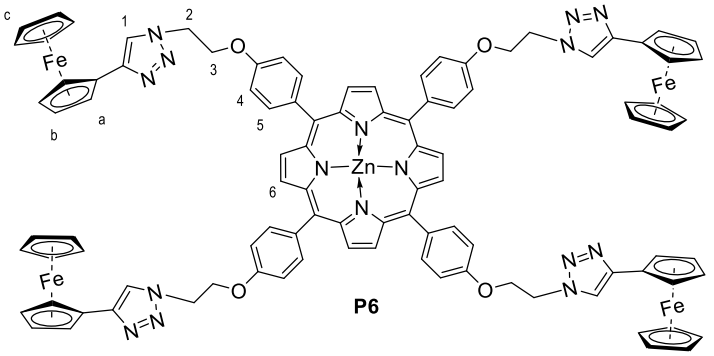

^{1}H NMR (500 MHz, pyridine-d5) δ (ppm): 9.19 (s, 8H, H_6), 8.48 (s, 4H, H_1), 8.25 (d, *J* = 8.3 Hz, 8H, H_4), 7.35 (d, *J* = 8.4 Hz, 8H, H_5), 5.09 (t, *J* = 5.0 Hz, 8H, H_3), 5.05 (t, *J* = 1.65 Hz, 8H, H_a), 4.74 (t, *J* = 5.0 Hz, 8H, H_2); 4.34 (t, *J* = 1.6 Hz, 8H, H_b), 4.17 (s, 20H, H_c). ^{13}C NMR (500 MHz, pyridine-d5) δ (ppm): 162.2, 158.1, 150.7, 146.8, 132.0, 121.3, 112.9, 76.8, 69.9, 68.8, 67.1, 49.9. MS (ESI): m/z calcd. For $C_{100}H_{80}Fe_4N_{16}O_4Zn$ = 1856.32, found $[M + 2H]^{2+}$ = 929.6.

6.3. UV-VIS AND DLS STUDIES

6.3.1. Preparation of mother solutions

Mother solutions of **P4**, **P6**, β-CD and β-CD dimer for the UV-vis and DLS studies were prepared as follows:

- 1.0 mM solution of **P4** in THF: 0.89 mg of **P4** were dissolved in 400 μL of THF.
- 0.73 mM solution of **P6** in THF/pyridine: 0.83 mg of **P6** were dissolved in a mixture of THF (450 μL) and pyridine (165 μL).
- 1.0 mM solution of β-CD in H_2O: 11.08 mg of β-CD were dissolved in 10 mL of Milli-Q H_2O.
- 1.0 mM solution of β-CD dimer in H_2O: 25.94 mg of β-CD dimer were dissolved in 10 mL of Milli-Q H_2O.

The mother solutions of **P4** and **P6** were prepared by weighing the solid product in a chromatography vial and then adding the solvent with a glass micro syringe.

The mother solutions of β-CD and β-CD dimer were prepared by weighing the solid product in a volumetric flask and then adding the solvent until the correct volume was reached.

6.3.2. UV-Vis and DLS studies

Studies of **P4** in water: The sample solutions were prepared by adding the proper amount of the 1 mM stock solution of **P4** in THF to a proper amount of water, β-CD or β-CD dimer aqueous solutions in 10 mL vials (with a glass micro syringe). The resulting mixtures were then magnetically stirred under vacuum for 1 min to evaporate THF co-solvent, by using an homemade stopper provided with a vacuum outlet connected to a membrane pump (~ 150 mbar). Afterwards, the UV-Vis and DLS measurements were consecutively performed on those samples, by transferring 2 mL of the prepared solutions to a 1 cm quartz cuvette. The UV-Vis and DLS measurements were performed on the freshly prepared samples (within 30 min), as well as at 24 h, and 48 h after solution preparation. A temperature scan experiment was also performed, where UV-Vis spectra were recorded every 5 ºC from 25 to 75 ºC, and then at 25 ºC again after cooling. DLS was measured at the beginning (at 25 ºC) and after the heating/cooling cycle, when the solution returned to 25 ºC. The following samples were prepared and studied as specified:

- 10 μM **P4** in water: 40 μL of 1mM **P4** solution in THF was added to 4 mL of Milli-Q H_2O.
- 10 μM **P4** + 20 μM β-CD: 40 μL of 1 mM **P4** solution in THF was added to 3.92 mL of H_2O and 80 μL of 1 mM β-CD solution.
- 10 μM **P4** + 40 μM β-CD: 40 μL of 1 mM **P4** solution in THF was added to 3.84 mL of H_2O and 160 μL of 1 mM β-CD solution.
- 10 μM **P4** + 200 μM β-CD: 40 μL of 1mM **P4** in THF solution was added to 3.20 mL of H_2O and 800 μL of 1 mM β-CD solution.

Studies with **P6**: The sample solutions of **P6** were prepared by adding the proper amount of the 0.73 mM stock solution of **P6** in THF/pyridine to 3 mL of Milli-Q water, β-CD or β-CD dimer aqueous solutions in a 10 mL vial. Then, 2 mL of those solutions were added to a 1 cm quartz cuvette for the UV-Vis and DLS measurements. The following samples were prepared:

- 10 μM mM of **P6** in water: 40 μL of 0.73 mM **P6** solution was added to 3 mL of H_2O.
- 10 μM **P6**+ 20 μM β-CD: 40 μL of 0.73 mM **P6** solution was added to 2.94 mL of H_2O, 60 μL of 1 mM β-CD solution.

- 10 μM **P6**+ 40 μM β-CD: 40 μL of 0.73 mM **P6** solution was added to 2.88 mL of H_2O, 120 μL of 1 mM β-CD solution.
- 10 μM **P6**+ 200 μM β-CD: 40 μL of 0.73 mM **P6** solution was added to 2.40 mL of H_2O, 600 μL of 1 mM β-CD solution.
- 10 μM **P6**+ 20 μM β-CD dimer: 40 μL of 0.73 mM **P6** solution was added to 2.94 mL of H_2O, 60 μL of 1 mM β-CD dimer solution.
- 10 μM **P6**+ 100 μM β-CD dimer: 40 μL of 0.73 mM **P6** solution was added to 2.7 mL of H_2O, 300 μL of 1 mM β-CD dimer solution.

7. CONCLUSIONS

In conclusion, in this TFG work we have:

- Successfully synthesized a novel Fc-functionalised zinc porphyrin, **P6**, through a convergent synthesis approach and using 'click' chemistry. The final product (~ 70 mg) has been characterised by ^{1}H NMR, ^{13}C NMR, and mass spectrometry.
- Optimised the synthesis of **P1**, having identified one of the main subproducts that formed when we initially used a reported protocol, adjusting the conditions to obtain a better yield.
- Studied the assembly behaviour of previously synthesised porphyrin **P4** in aqueous solutions, both alone and in the presence of β-CD, by UV-Vis and DLS measurements. The results show that **P4** self-assembles in aqueous solution, where the presence of β-CD affects the size and structure of the assemblies, as suggested by changes in their hydrodynamic diameter and UV-Vis spectrum. In addition, we found that these assemblies do not change significantly with time, or upon a heating/cooling cycle.
- Studied the assembly behaviour of the novel porphyrin **P6** in aqueous solutions, alone and in the presence of β-CD or β-CD dimer, by UV-Vis and DLS measurements. The results show that **P6** self-assembles into larger aggregated structures than **P4**, which do not appear to be affected by the presence of β-CD (in contrast to **P4**). However, in the presence of β-CD dimer, the appearance of an aggregate population with higher hydrodynamic diameter was observed by DLS. Further studies need to be carried out to determine if this observation can be ascribed to the formation of extended supramolecular networks.

8. REFERENCES AND NOTES

1. Steed, J. W. & Atwood, J. L. *Supramolecular Chemistry*. (John Wiley & Sons, 2013).
2. Yaghi, O. M. *et al.* Reticular synthesis and the design of new materials. *Nature* **423**, 705–714 (2003).
3. Côté, A. P. *et al.* Porous, Crystalline, Covalent Organic Frameworks. *Science* **310**, 1166–1170 (2005).
4. Sánchez-González, E., Ying Tsang, M., Troyano, J., A. Craig, G. & Furukawa, S. Assembling metal–organic cages as porous materials. *Chem. Soc. Rev.* **51**, 4876–4889 (2022).
5. Hosono, N. & Kitagawa, S. Modular Design of Porous Soft Materials via Self-Organization of Metal–Organic Cages. *Acc. Chem. Res.* **51**, 2437–2446 (2018).
6. Tian, J., Wang, H., Zhang, D.-W., Liu, Y. & Li, Z.-T. Supramolecular organic frameworks (SOFs): homogeneous regular 2D and 3D pores in water. *Natl. Sci. Rev.* **4**, 426–436 (2017).
7. Shen, M.-N. *et al.* Recent progress on the construction of supramolecular organic frameworks based on macrocyclic hosts. *Mol. Syst. Des. Eng.* **7**, 1570–1587 (2022).
8. Tian, J., Chen, L., Zhang, D.-W., Liu, Y. & Li, Z.-T. Supramolecular organic frameworks: engineering periodicity in water through host–guest chemistry. *Chem. Commun.* **52**, 6351–6362 (2016).
9. Li, Z.-T., Yu, S.-B., Liu, Y., Tian, J. & Zhang, D.-W. Supramolecular Organic Frameworks: Exploring Water-Soluble, Regular Nanopores for Biomedical Applications. *Acc. Chem. Res.* **55**, 2316–2325 (2022).
10. Yang, B. *et al.* Self-Assembly of a Bilayer 2D Supramolecular Organic Framework in Water. *Angew. Chem.* **133**, 26472–26479 (2021).
11. Liu, J. *et al.* Aggregation-Induced Emission Supramolecular Organic Framework (AIE SOF) Gels Constructed from Supramolecular Polymer Networks Based on Tripodal Pillar[5]arene for Fluorescence Detection and Efficient Removal of Various Analytes. *ACS Sustain. Chem. Eng.* **7**, 11999–12007 (2019).
12. Lee, H.-J., Kim, H.-J., Lee, E.-C., Kim, J. & Park, S. Y. Highly Luminescent and Water-Soluble Two-Dimensional Supramolecular Organic Framework: All-Organic Photosensitizer Template for Visible-Light-Driven Hydrogen Evolution from Water. *Chem. – Asian J.* **13**, 390–394 (2018).
13. Rossum, S. A. P. van, Tena-Solsona, M., Esch, J. H. van, Eelkema, R. & Boekhoven, J. Dissipative out-of-equilibrium assembly of man-made supramolecular materials. *Chem. Soc. Rev.* **46**, 5519–5535 (2017).
14. Rieß, B., Grötsch, R. K. & Boekhoven, J. The Design of Dissipative Molecular Assemblies Driven by Chemical Reaction Cycles. *Chem* **6**, 552–578 (2020).
15. De, S. & Klajn, R. Dissipative Self-Assembly Driven by the Consumption of Chemical Fuels. *Adv. Mater.* **30**, 1706750 (2018).
16. van Ravensteijn, B. G. P., Voets, I. K., Kegel, W. K. & Eelkema, R. Out-of-Equilibrium Colloidal Assembly Driven by Chemical Reaction Networks. *Langmuir* **36**, 10639–10656 (2020).
17. Boekhoven, J., Hendriksen, W. E., Koper, G. J., Eelkema, R. & van Esch, J. H. Transient assembly of active materials fueled by a chemical reaction. *Science* **349**, 1075–1079 (2015).
18. Maiti, S., Fortunati, I., Ferrante, C., Scrimin, P. & Prins, L. J. Dissipative self-assembly of vesicular nanoreactors. *Nat. Chem.* **8**, 725–731 (2016).

19. Sorrenti, A., Leira-Iglesias, J., Sato, A. & Hermans, T. M. Non-equilibrium steady states in supramolecular polymerization. *Nat. Commun.* **8**, 15899 (2017).
20. Dong, S., Zheng, B., Wang, F. & Huang, F. Supramolecular Polymers Constructed from Macrocycle-Based Host–Guest Molecular Recognition Motifs. *Acc. Chem. Res.* **47**, 1982–1994 (2014).
21. Ma, X. & Zhao, Y. Biomedical Applications of Supramolecular Systems Based on Host–Guest Interactions. *Chem. Rev.* **115**, 7794–7839 (2015).
22. Harada, A., Takashima, Y. & Nakahata, M. Supramolecular Polymeric Materials via Cyclodextrin–Guest Interactions. *Acc. Chem. Res.* **47**, 2128–2140 (2014).
23. Peng, L., Feng, A., Huo, M. & Yuan, J. Ferrocene-based supramolecular structures and their applications in electrochemical responsive systems. *Chem Commun* **50**, 13005–13014 (2014).
24. Gu, H. *et al.* Redox-stimuli-responsive drug delivery systems with supramolecular ferrocenyl-containing polymers for controlled release. *Coord. Chem. Rev.* **364**, 51–85 (2018).
25. González Garcia, Guillem. *TFG project*. (2023).
26. Bragina, N. A., Mishkina, K. A., Formirovsky, K. A. & Mironov, A. F. Synthesis of Amphiphilic meso-Aryl-porphyrins in Organic Solvents and Aqueous Micellar Medium. *Macroheterocycles* **4**, 116–121 (2011).
27. Rumyantseva, V. D., Gorshkova, A. S. & Mironov, A. F. Improved Method of 5,10,15,20-Tetrakis(4-hydroxyphenyl)porphyrins Synthesis. *Macroheterocycles* **6**, 59–61 (2013).
28. Choi, H., Shirley, H. J., Hume, P. A., Brimble, M. A. & Furkert, D. P. Unexpected Direct Synthesis of N-Vinyl Amides through Vinyl Azide–Enolate [3+ 2] Cycloaddition. *Angew. Chem.* **129**, 7528–7532 (2017).
29. Hou, Z., Dehaen, W., Lyskawa, J., Woisel, P. & Hoogenboom, R. A supramolecular miktoarm star polymer based on porphyrin metal complexation in water. *Chem. Commun.* **53**, 8423–8426 (2017).
30. Sun, Z.-Z. *et al.* Preparation and the biodistribution study of [131I]-5,10,15,20-tetrakis(4-hydroxyphenyl)porphyrin and 5-(4-aminophenyl)-10,15,20-triphenylporphyrin. *J. Radioanal. Nucl. Chem.* **302**, 123–130 (2014).
31. Gao, Y. *et al.* Formation Mechanism of Iodinated Aromatic Disinfection Byproducts: Acid Catalysis with H_2OI^+. *Environ. Sci. Technol.* **56**, 1791–1800 (2022).

9. ACRONYMS

MOF(s)	Metal-Organic Framework(s)
COF(s)	Covalent Organic Framework(s)
SOF(s)	Supramolecular Organic Framework(s)
CD(s)	Cyclodextrin(s)
Fc	Ferrocene
TEG	Tetraethylene Glycol
CB[8]	Cucurbit[8]uril
DLS	Dynamic Light Scattering
DSA	Dissipative Self-Assembly
TLC	Thin-Layer Chromatography
NMR	Nuclear Magnetic Resonance
ESI-MS	Electrospray Ionization-Mass Spectrometry
UV-Vis	Ultraviolet Visible Spectroscopy
LC-MS	Liquid Chromatography-Mass Spectrometry
DMSO	Dimethyl sulfoxide
THF	Tetrahydrofuran
DCM	Dichloromethane
DMF	Dimethylformamide

APPENDICES

APPENDIX 1: UV-VIS SPECTRA

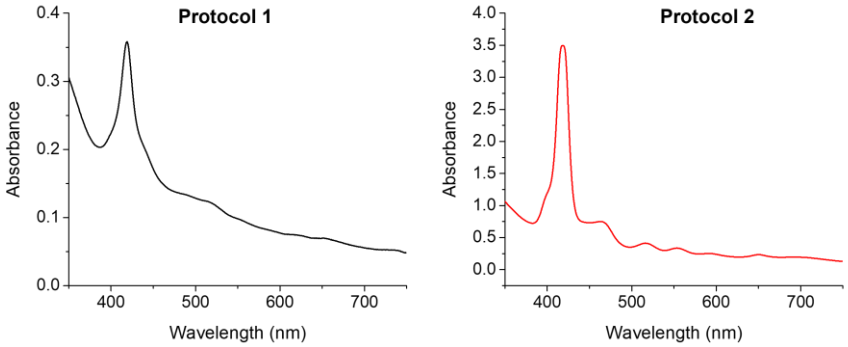

UV-vis spectra of the crude reaction mixture in the synthesis of **P1**

APPENDIX 2: TEMPERATURE SCAN EXPERIMENTS

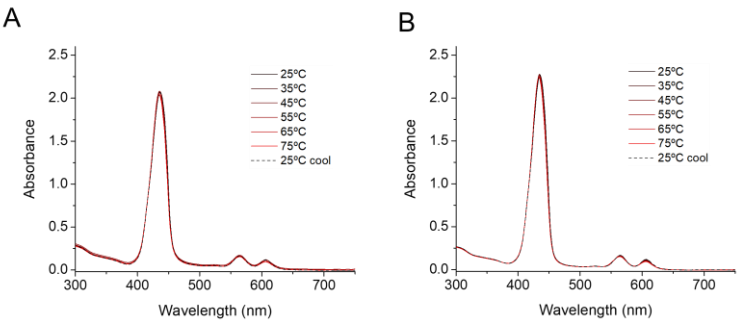

UV-Vis spectra in water of: A) **P4** (10 μM); and B) **P4** (10 μM) + βCD (40 μM) at different temperatures along a heating/cooling cycle.

APPENDIX 3: DLS DATA 1

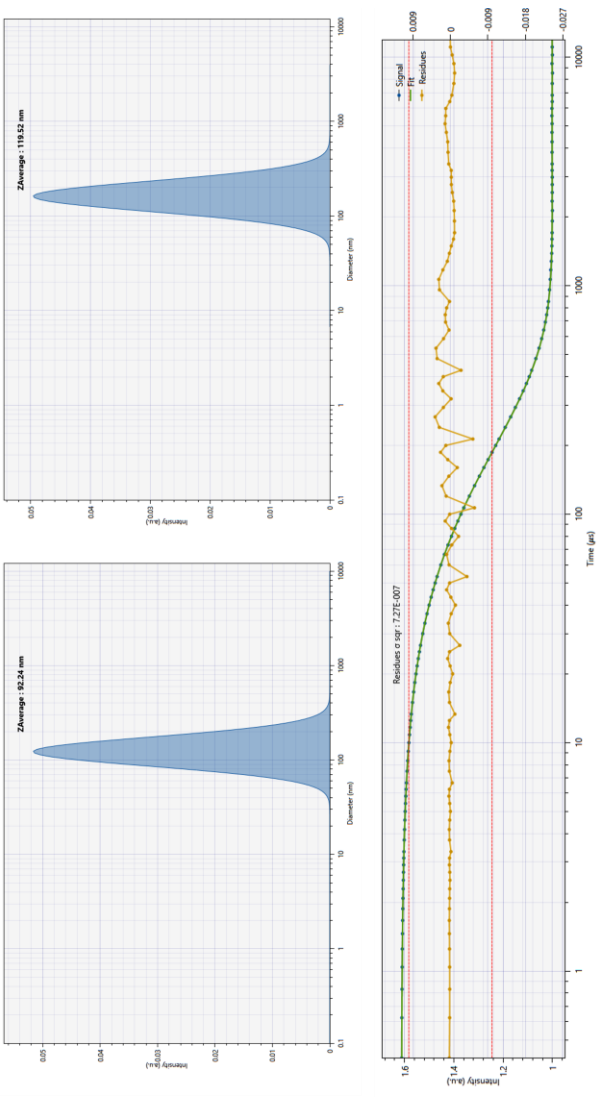

Top: examples of size distributions in samples of **P4**. Bottom: examples of good fitting of the autocorrelation function (the orange residues are within the red margins)

APPENDIX 4: DLS DATA 2

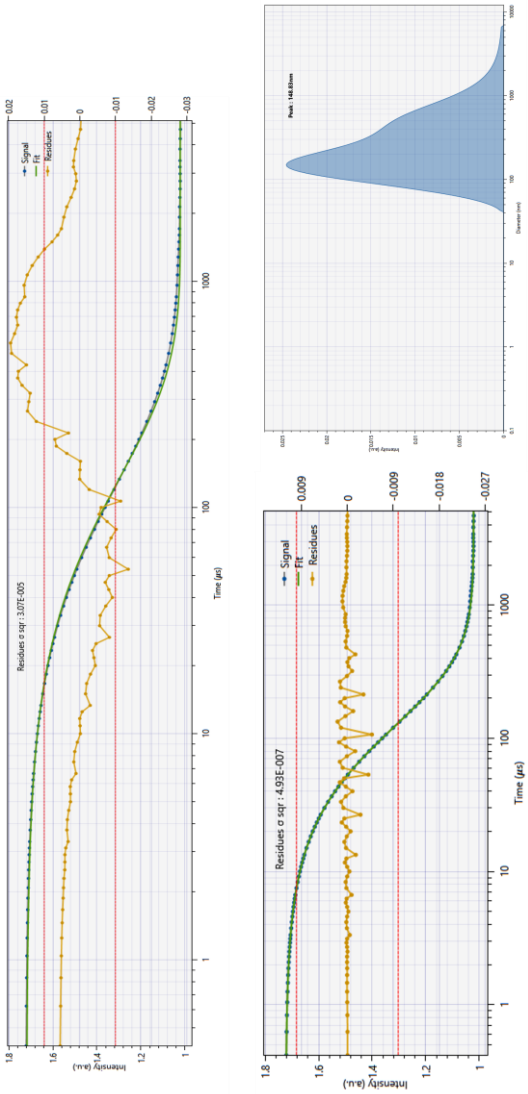

Top: poor fitting when considering a single population of scatterers (the orange residues are beyond the red margins). Bottom: improved fitting when considering two populations.